


New Donor–Acceptor Oligoimides for High-Performance Nonvolatile Memory Devices

Wen-Ya Lee,^{†,‡,||} Tadanori Kurosawa,^{§,||} Shiang-Tai Lin,[†] Tomoya Higashihara,[§] Mitsuru Ueda,^{*,§} and Wen-Chang Chen^{*,†,‡}

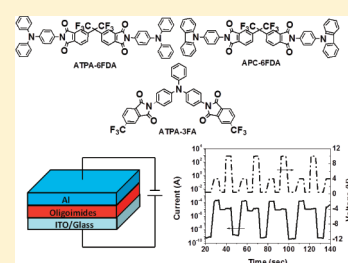
[†]Department of Chemical Engineering and [‡]Institute of Polymer Science and Engineering, National Taiwan University, Taipei 106, Taiwan

[§]Department of Organic and Polymeric Materials, Tokyo Institute of Technology, Tokyo 152-8552, Japan

 Supporting Information

ABSTRACT: We report the synthesis, optoelectronic properties, and electrical switching memory characteristics of three new donor–acceptor oligoimides consisting of the electron-donating moieties (triphenylamine or carbazole) and electron-withdrawing phthalimide moieties. The influence of different donor (D)–acceptor (A) arrangements, including D-A-D and A-D-A structures, on the electrical properties was explored. Devices based on D-A-D oligoimides revealed a reversible nonvolatile negative-differential-resistance (NDR) characteristic and excellent stability during operation. Without applying voltage stress, the on and off states of the devices showed no obvious degradation for an operation time of 10 s and 10⁸ read pulses. However, the devices prepared from the A-D-A oligoimide showed only the insulating properties. The different memory characteristic was probably because the terminal donor moieties in the D-A-D structure might facilitate the injection and transporting of the holes. Besides, the D-A-D oligoimide with triphenylamine groups exhibited an on/off ratio of 10⁴, 2 orders of magnitude higher than that with carbazole groups. The mechanism related to electrical switching properties was elucidated through molecular simulation. Thus the significance of D-A-D structure on tuning memory characteristics for memory device applications was revealed.

KEYWORDS: oligoimide, donor–acceptor, memory, NDR, resistor type



INTRODUCTION

Organic materials have been extensively investigated recently for data storage devices due to low cost, structural flexibility, and three-dimensional stacking capability.¹ A wide range of organic materials containing electron-donating (D) and electron-accepting (A) groups, including functional polyimides,² conjugated polymers,³ conjugated diblock copolymers,⁴ nonconjugated polymers with pendant conjugated donor/acceptor moieties,⁵ oligomers,⁶ polymer–graphene complex,⁷ polymer/fullerene blends,⁸ and organic molecules blended with nanoparticles⁹ have been reported for the application of memory devices. Charge transfer between donor and acceptor moieties of the polyimides enhanced the conductivity of the thin films and was responsible for the resulting memory characteristics.^{1a,2a–2e} Switching between high- and low-conductive state (on and off) of donor–acceptor polymers under applied voltages is important for data storage devices.

Donor–acceptor polyimides are one of the most promising candidates for memory device applications, since they not only have good electrical properties for charge storage but also possess excellent thermal stability (higher than 500 °C) and chemical etching resistance. Various memory types based on the polyimides were demonstrated, including dynamic random access memory (DRAM),^{2d,i} static random access memory (SRAM),^{2a,f} write-once-read-many (WORM),^{2c,j} and flash memory.^{2g} Most studies on the memory behaviors of imide-based materials

mainly focused on the effects of the donor/acceptor chemical structures of polyimides on the electrical switching behavior. However, the imide molecules for the memory device application are rarely studied.

The electrical switching behaviors of several D-A oligomers have been reported in the literature.⁶ Tetracyanoquinodimethane (TCNQ)–Cu complexes, in which TCNQ and Cu were used as acceptor and donor moieties, respectively, exhibited electrical switching.^{6a} This switching was elucidated by the electrochemical formation of the Cu filaments.^{6b} In comparison to the heterogeneous organic–metal complexes, all organic D-A molecules could provide more uniform properties.^{6c–e} Song and co-workers^{6d} employed the molecules containing electron-donating triphenylamine and electron-accepting cyanovinyl moieties for the memory device applications, in which triphenylamine provided a better hole transporting ability for improving the on/off current ratios. Later, they demonstrated that the different architecture of the cyanide-substituted triphenylamine molecules affected the on/off ratio and reversibility of their memory devices significantly.^{6e} The devices prepared from the D- π -A- π -D molecules performed good write-read-erase characteristics.^{6e} In contrast, the A- π -D- π -A molecules exhibited

Received: June 13, 2011

Revised: September 1, 2011

Published: September 21, 2011

a relatively low on/off ratio and irreversible switching behavior. It was suggested that the arrangement of the donor and acceptor moieties affected the electrical switching characteristics significantly.

In this paper, we report the synthesis, optoelectronic properties, and electrical switching memory characteristics of three new donor–acceptor oligoimides, containing the electron-donating moieties triphenylamine or carbazole and electron-withdrawing phthalimide moieties. Both triphenylamine and carbazole groups were explored intensively for data storage devices, since they possessed excellent hole-transporting abilities. The rigid bridge of carbazole may induce different molecular conformations and electrical performance from the triphenylamine. The memory device was fabricated on the indium tin oxide (ITO) coated glass with the configuration ITO/oligoimides/Al. The influence of two donor–acceptor arrangements (D-A-D and A-D-A structures) on the electrical properties was also studied and elucidated through molecular simulation. The experimental results suggested that the D-A-D oligoimide-based devices revealed the reversible nonvolatile negative-differential-resistance (NDR) characteristics with on/off ratios of 10^2 – 10^4 and excellent stability during operation. However, the devices prepared from the A-D-A oligoimide showed only the insulating properties. This study provided new strategies for the molecular design of donor–acceptor oligomers for advanced memory applications.

EXPERIMENTAL SECTION

Materials. 4-Fluoronitrobenzene and 4-trifluoromethylphthalic acid were purchased from Sigma–Aldrich Corp. and used as received. Tetrabutylammonium perchlorate (TBAP, from TCI) was recrystallized twice from ethyl acetate and then dried in vacuo prior to use. 4,4'-(Hexafluoroisopropylidene)diphthalic anhydride (6FDA, from TCI) was purified by sublimation. Dehydrated tetrahydrofuran (THF), dehydrated *N,N*-dimethylacetamide (DMAc), anhydrous potassium carbonate, acetic anhydride, and cyclohexane were purchased from Wako, Japan. Dehydrated THF (Wako, stabilizer-free, 99.5%) was distilled from its sodium naphthalenide solution under nitrogen. All other compounds were purchased from TCI and used without further purification.

Synthesis of 4-Nitrotriphenylamine (NTPA). Diphenylamine (1.69 g, 10.0 mmol) was added to a solution of sodium hydride (0.375 g, 15.6 mmol) in dehydrated DMAc (10 mL). The solution was stirred at room temperature for 30 min and cooled to 0 °C. 4-Fluoronitrobenzene (1.69 g, 12.0 mmol) in dehydrated DMAc (10 mL) was added dropwise to this mixture. After the addition was complete, the mixture was stirred at 100 °C for 1 h. Then the mixture was cooled to room temperature and poured into a cold dilute hydrochloric acid solution. The crude product was collected by filtration and recrystallized from 2-propanol and water to give orange crystals (2.79 g) in 92% yield. IR (KBr) ν (cm^{-1}) 1581, 1315 (NO_2 stretching). ^1H NMR (300 MHz, $\text{DMSO-}d_6$, δ , ppm) 8.07 (d, $J = 9.3$ Hz, ArH, 2H), 7.45 (t, $J = 7.8$ Hz, ArH, 4H), 7.31–7.25 (m, ArH, 6H), 6.80 (d, $J = 9.6$ Hz, ArH, 2H).

Synthesis of *N*-(4-Nitrophenyl)carbazole (NPC). A 100-mL two necked flask equipped with a magnetic stirrer, a nitrogen inlet, a Dean–Stark trap, and a condenser was charged with carbazole (3.34 g, 20.0 mmol), K_2CO_3 (3.04 g, 22.0 mmol), dehydrated DMAc (40 mL), and cyclohexane (15 mL). The mixture was heated to 120 °C for 4 h under nitrogen to facilitate dehydration. After complete removal of water, the residual cyclohexane was distilled off and 4-fluoronitrobenzene (2.33 mL, 22.0 mmol) was then added. The mixture was heated to 160 °C and maintained at this temperature for 2 h. Then the mixture was

poured into 1 M hydrochloric acid solution to give a pale greenish-yellow solid. The crude product was purified by recrystallization from toluene and hexane to give pale greenish-yellow crystals (4.50 g) in 78% yield. IR (KBr) ν (cm^{-1}) 1592, 1330 (NO_2 stretching). ^1H NMR (300 MHz, $\text{DMSO-}d_6$, δ , ppm) 8.48 (d, $J = 8.7$ Hz, ArH, 2H), 8.25 (d, $J = 8.1$ Hz, ArH, 2H), 7.93 (d, $J = 9.0$ Hz, ArH, 2H), 7.54 (d, $J = 8.4$ Hz, ArH, 2H), 7.46 (t, $J = 6.9$ Hz, ArH, 2H), 7.34 (t, $J = 7.2$, ArH, 2H).

Synthesis of 4,4'-Dinitrotriphenylamine (DNTPA). DNTPA was synthesized according to a similar procedure as NTPA, from *N*-(4-nitrophenyl)aniline^{2f} and 4-fluoronitrobenzene. The product was purified by recrystallization from ethanol and water. The yield of DNTPA was 92%. IR (KBr) ν (cm^{-1}) 1581, 1342 (NO_2 stretching). ^1H NMR (300 MHz, $\text{DMSO-}d_6$, δ , ppm) 8.19 (d, $J = 9.3$ Hz, ArH, 4H), 7.51 (t, $J = 7.5$ Hz, ArH, 2H), 7.37 (t, $J = 6.9$ Hz, ArH, 2H), 7.27 (d, $J = 7.5$ Hz, ArH, 2H), 7.20 (d, $J = 9.0$ Hz, ArH, 4H).

Synthesis of 4-Aminotriphenylamine (ATPA). NTPA (1.45 g, 5.00 mmol) and palladium on activated carbon (Pd/C) (0.0725 g) was dissolved in ethanol (10 mL) and the solution was refluxed. Hydrazine monohydrate (1.5 mL) was added dropwise, and the mixture was stirred at this temperature for 12 h. The reaction solution was immediately filtered through Celite before cooling down to room temperature due to the low solubility of ATPA in ethanol. The filtrate was concentrated and poured into water. The precipitate was collected by filtration and purified by recrystallization from ethanol to yield white crystals (0.726 g) in 56% yield. IR (KBr) ν (cm^{-1}) 3460, 3375 (N–H stretching). ^1H NMR (300 MHz, $\text{DMSO-}d_6$, δ , ppm) 7.19 (t, $J = 8.1$ Hz, ArH, 2H), 6.91–6.85 (m, ArH, 6H), 6.80 (d, $J = 8.4$ Hz, ArH, 2H), 6.57 (d, $J = 8.7$ Hz, ArH, 2H), 5.09 (s, N–H, 2H).

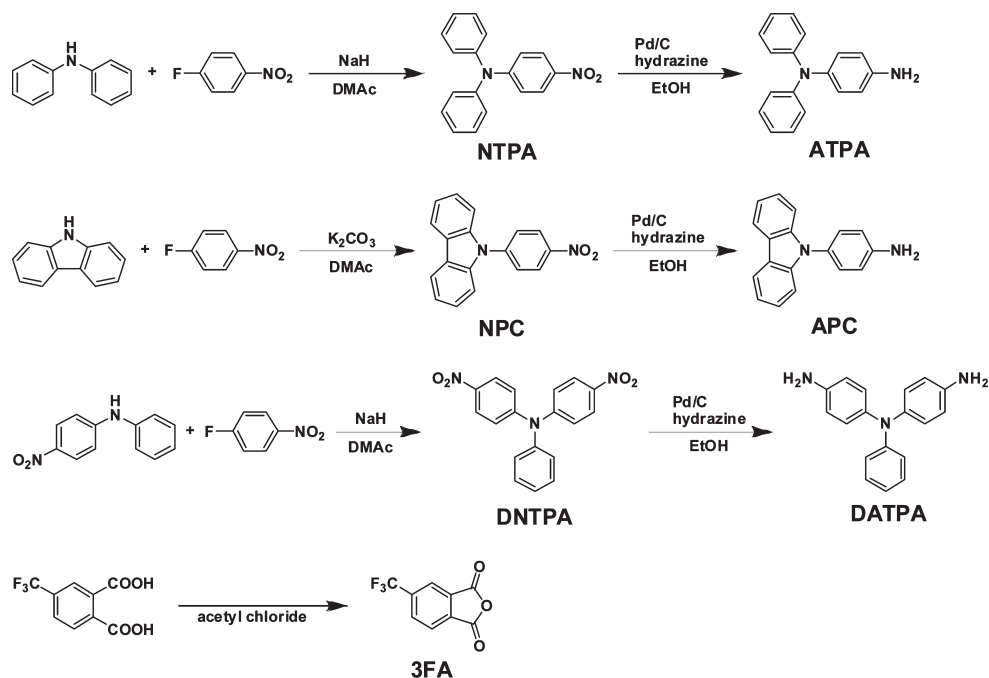
Synthesis of *N*-(4-Aminophenyl)carbazole (APC). To a refluxed solution of NPC (1.44 g, 5.00 mmol) and Pd/C (0.0720 g) in ethanol (10 mL) was added dropwise hydrazine monohydrate (1.5 mL). The mixture was refluxed for 4 h and cooled to room temperature. Pd/C was removed by filtration through Celite and the filtrate was concentrated to give APC as a clear viscous liquid (1.24 g) in 96% yield. IR (KBr) ν (cm^{-1}) 3460, 3379 (N–H stretching). ^1H NMR (300 MHz, $\text{DMSO-}d_6$, δ , ppm) 8.19 (d, $J = 8.1$ Hz, ArH, 2H), 7.40 (t, $J = 7.5$ Hz, ArH, 2H), 7.27–7.21 (m, ArH, 4H), 7.18 (d, $J = 9.0$ Hz, ArH, 2H), 6.81 (d, $J = 8.4$ Hz, ArH, 2H), 5.35 (s, N–H, 2H).

Synthesis of 4,4'-Diaminotriphenylamine (DATPA). Starting from DNTPA, DATPA was synthesized by a similar procedure as ATPA. The crude product was purified by recrystallization from ethanol and water in 77% yield. IR (KBr) ν (cm^{-1}) 3428, 3347 (N–H stretching). ^1H NMR (300 MHz, $\text{DMSO-}d_6$, δ , ppm) 7.04 (t, $J = 8.7$ Hz, ArH, 2H), 6.80 (d, $J = 8.4$ Hz, ArH, 4H), 6.65–6.57 (m, ArH, 3H), 6.53 (d, $J = 8.7$ Hz, ArH, 4H), 4.98 (s, N–H, 4H).

Synthesis of 4-Trifluoromethylphthalic Anhydride (3FA). 4-Trifluoromethylphthalic acid (7.02 g, 30.0 mmol) was dissolved in acetyl chloride (15 mL) and the mixture was refluxed for 16 h. After the reaction, acetyl chloride was distilled off and the residual solid was purified by sublimation to yield a white crystal (6.17 g) in 95% yield. IR (KBr) ν (cm^{-1}) 1867, 1774 (C=O stretching), 918 (C–CO–O–CO–C stretching). ^1H NMR (300 MHz, $\text{DMSO-}d_6$, δ , ppm) 8.51 (s, ArH, 1H), 8.37 (d, $J = 7.8$ Hz, ArH, 1H), 8.29 (d, $J = 8.1$ Hz, ArH, 1H).

Synthesis of 4,4'-Hexafluoroisopropylidenebis[4-(*N,N*-diphenylamino)phenyl phthalimide] (ATPA-6FDA). 6FDA (0.555 g, 1.25 mmol) was added to a solution of ATPA (0.651 g, 2.50 mmol) in dehydrated THF (3 mL) under nitrogen. The solution was stirred for 1 h and then THF was evaporated. The residual solid was dissolved in acetic anhydride (5 mL) and refluxed for 4 h. After cooling to room temperature, the precipitate was collected by filtration and washed with water to give an orange powder (1.02 g) in 88% yield. The obtained product was used without further purification. IR (KBr) ν (cm^{-1}) 1781, 1720 (C=O stretching), 1381 (C–N stretching). ^1H

Scheme 1. Synthetic Routes for ATPA, APC, DATPA, and 3FA



NMR (300 MHz, DMSO- d_6 , δ , ppm) 8.17 (d, J = 8.7 Hz, ArH, 2H), 7.94 (d, J = 8.1, ArH, 2H), 7.74 (s, ArH, 2H), 7.37–7.30 (m, ArH, 12H), 7.12–7.04 (m, ArH, 16H). ^{13}C NMR (75 MHz, DMSO- d_6 , δ , ppm) 167.0, 166.9, 148.5, 148.3, 148.2, 147.9, 133.9, 133.5, 130.5, 129.0, 128.8, 126.5, 125.5, 125.1, 124.5, 123.3, 94.95. Anal. Calcd for $\text{C}_{55}\text{H}_{34}\text{N}_4\text{F}_6\text{O}_4$: C, 71.1; H, 3.69; N, 6.03. Found: C, 70.7; H, 3.85; N, 5.98.

Synthesis of 4,4'-Hexafluoroisopropylidenebis[4-(carbazol-9-yl)phenyl phthalimide] (APC-6FDA). APC-6FDA was synthesized according to a similar procedure as ATPA-6FDA. The yield of APC-6FDA was 74%. IR (KBr) ν (cm^{-1}) 1785, 1724 (C=O stretching), 1357 (C–N stretching). ^1H NMR (300 MHz, DMSO- d_6 , δ , ppm) 8.26–8.23 (m, ArH, 6H), 8.03 (d, J = 7.8 Hz, ArH, 2H), 7.88 (s, ArH, 2H), 7.81 (s, ArH, 8H), 7.48–7.46 (m, ArH, 8H), 7.35–7.29 (m, ArH, 4H). ^{13}C NMR (75 MHz, DMSO- d_6 , δ , ppm) 167.7, 166.9, 166.8, 157.2, 155.7, 151.0, 148.4, 141.6, 141.0, 137.6, 133.6, 131.6, 129.8, 128.0, 127.2, 123.9, 121.4, 121.1, 110.6. Anal. Calcd for $\text{C}_{55}\text{H}_{30}\text{N}_4\text{F}_6\text{O}_4$: C, 71.4; H, 3.27; N, 6.06. Found: C, 71.2; H, 3.34; N, 5.99.

Synthesis of *N,N'*-[(Phenylimino)di-4,1-phenylene]bis(5-trifluoromethyl phthalimide) (APTA-3FA). To a solution of DATP (1.11 g, 4.03 mmol) in dehydrated THF (20 mL) was added 4-trifluoromethylphthalic anhydride (1.94 g, 9.00 mmol). The mixture was stirred for 1 h and then THF was evaporated. The residual solid was dissolved in 1,3-dimethyl-2-imidazolidinone (DMI) (10 mL) and refluxed for 4 h. After cooling to room temperature, the solution was poured into water. The precipitate was collected by filtration and excess 3FA was removed by sublimation to give 2.61 g of an orange powder (2.61 g) in 96% yield, mp 219 °C (DSC peak). IR (KBr) ν (cm^{-1}) 1782, 1724 (C=O stretching), 1384 (C–N stretching). ^1H NMR (300 MHz, DMSO- d_6 , δ , ppm) 8.28–8.26 (m, ArH, 4H), 8.17 (d, J = 8.4 Hz, ArH, 2H), 7.43–7.38 (m, ArH, 6H), 7.20–7.17 (m, ArH, 7H). ^{13}C NMR (75 MHz, DMSO- d_6 , δ , ppm) 166.3, 166.2, 147.2, 135.5, 134.8, 134.4, 133.1, 132.0, 130.2, 128.7, 126.5, 125.6, 124.8, 123.7, 120.4. Anal. Calcd for $\text{C}_{36}\text{H}_{19}\text{N}_3\text{F}_6\text{O}_4$: C, 64.39; H, 2.85; N, 6.28. Found: C, 64.47; H, 3.03; N, 6.28.

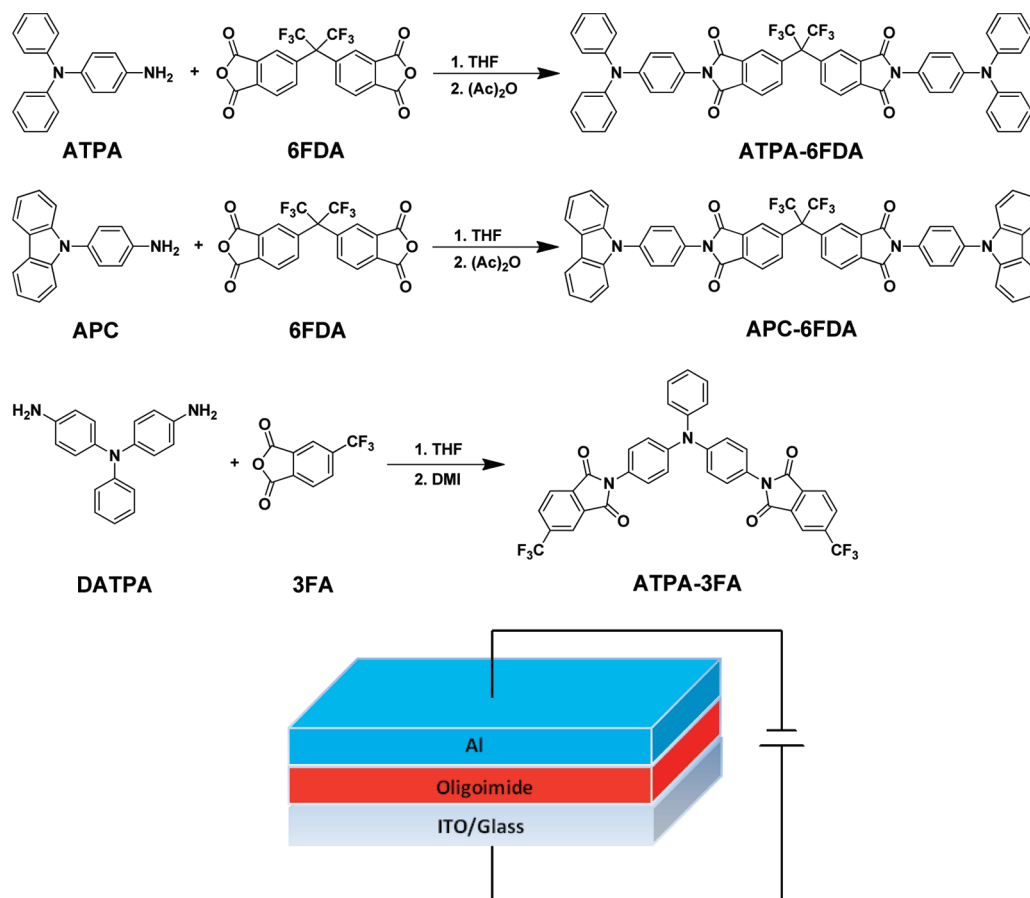
Characterizations. NMR spectra were recorded on a Bruker DPX-300S spectrometer at the resonant frequencies at 300 MHz for ^1H and

75 MHz for ^{13}C nuclei with deuterated dimethyl sulfoxide (DMSO- d_6) as the solvent and tetramethylsilane as the reference. Fourier transform infrared (FT-IR) spectra were measured by a Horiba FT-120 Fourier transform spectrophotometer. Elemental analyses were performed on a Yanaco MT-6 CHN recorder elemental analysis instrument. Thermal properties were estimated from a Seiko TG/DTA 6300 thermogravimetric analysis system (TGA) and a TA Instruments DSC-Q100 differential scanning calorimeter (DSC) under a nitrogen atmosphere at a heating rate of 10 and 6 °C/min, respectively. Cyclic voltammetry was performed with the use of a three-electrode cell in which ITO (polymer film area was about $0.7 \times 0.5 \text{ cm}^2$) was used as a working electrode. A platinum wire was used as an auxiliary electrode. All cell potentials were taken with the use of a Ag/AgCl, KCl (saturated) reference electrode. UV–vis absorption spectra were measured with a Hitachi U4100 UV–vis–NIR spectrophotometer. The thickness of the polymer film was measured with a microfigure measuring instrument (Surfcoorder ET3000, Kosaka Laboratory Ltd.). Atomic force microscopy (AFM) measurements were obtained with a NanoScope IIIa AFM (Digital Instruments, Santa Barbara, CA) at room temperature. Commercial silicon cantilevers (Nanosensors, Germany) with typical spring constants of $15 \text{ N} \cdot \text{m}^{-1}$ were used to operate the AFM in tapping mode.

Fabrication and Characterization of Memory Devices. The memory device was fabricated on ITO-coated glass with the configuration ITO/oligoimides/Al. Before deposition of the organic layer, the ITO glass was precleaned by ultrasonication with water, acetone, and 2-propanol, each for 15 min. The layers of the oligoimides were vapor-deposited at a rate of $0.5 \text{ \AA} \cdot \text{s}^{-1}$ under a pressure of around 1×10^{-6} Torr to their target thickness (80 nm) as determined in situ by a calibrated quartz crystal microbalance (QCM). A 300-nm-thick Al electrode, $0.5 \times 0.5 \text{ mm}^2$, was thermally evaporated through the shadow mask at a pressure of 8×10^{-7} Torr with a uniform depositing rate of $2 \text{ \AA} \cdot \text{s}^{-1}$. The electrical characteristics of memory device were measured with a Keithley 4200 semiconductor parametric analyzer. All electronic measurements were performed in a N_2 -filled glovebox.

Computational Methodology. Theoretical molecular simulation of the oligoimides were calculated through the Gaussian 03 program package.¹⁰ Density functional theory (DFT) method, using Becke's

Scheme 2. Synthetic Routes for ATPA-6FDA, APC-6FDA, and ATPA-3FA and Their Memory Devices



three-parameter functional with the Lee, Yang, and Parr correlation functional method (B3LYP) with 6-31G(d), was exploited for the optimization of ground-state molecular geometry, electrostatic potential (ESP), and electronic properties.

RESULTS AND DISCUSSION

Synthesis of Oligoimides. The synthesis of amino compounds (ATPA, APC, and DATPA) is shown in Scheme 1. First the precursory nitro compounds (NTPA, NPC, and DNTPA) were prepared by aromatic nucleophilic substitution reactions between 4-fluoronitrobenzene and diphenylamine, carbazole, or *N*-(4-nitrophenyl)aniline.^{2f} Then NTPA, NPC, and DNTPA were converted to ATPA, APC, and DATPA, respectively, by Pd-catalyzed reduction. The disappearance of characteristic absorption peaks around 1580 and 1330 cm^{-1} due to the nitro groups and the appearance of characteristic peaks around 3450 and 3360 cm^{-1} assigned to the amino groups in the FT-IR spectra indicate complete reduction of NTPA, NPC, and DNTPA to ATPA, APC, and DATPA, respectively. The successful synthesis of these amino compounds was also confirmed by ^1H NMR. The signals at 5.09, 5.35, and 4.98 ppm were assigned to the amino groups of ATPA, APC, and DATPA, respectively. 3FA was synthesized by treatment of 4-trifluoromethylphthalic acid with acetyl chloride, as shown in Scheme 1. Formation of 3FA was also confirmed by the FT-IR and ^1H NMR spectra.

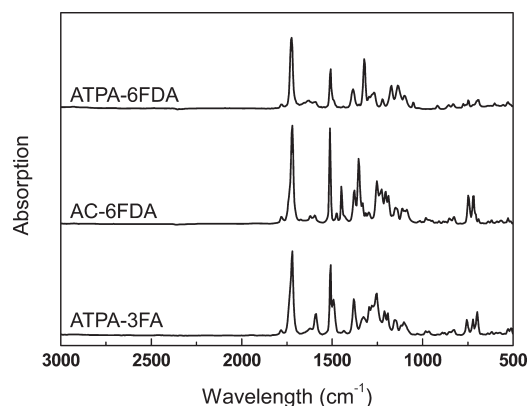


Figure 1. FT-IR spectra of ATPA-6FDA, APC-6FDA, and ATPA-3FA.

A series of imide compounds (ATPA-6FDA, APC-6FDA, and ATPA-3FA) were prepared by the condensation reaction of amino compounds (ATPA, APC, and DATPA) and acid anhydrides (6FDA and 3FA) in two steps, as shown in Scheme 2. First, the amino compounds and acid anhydrides were mixed in THF under nitrogen to yield amic acid solutions. Then, chemical imidization in acetic anhydride was carried out for the preparation of ATPA-6FDA and APC-6FDA. Both imide compounds were obtained as precipitates and used without further purification. For preparation of ATPA-3FA, thermal imidization was

performed in DMI because of high solubility of ATPA-3FA in acetic anhydride, and excess 3FA was removed by sublimation. The desirable structures of all imide compounds were confirmed by FT-IR spectra, which showed the characteristic peaks of imide groups at around 1780 cm^{-1} (asymmetrical stretching of carbonyl groups) and 1720 cm^{-1} (symmetrical stretching of carbonyl groups), and the C–N bond at around 1380 cm^{-1} , as presented in Figure 1. Moreover, the formation of ATPA-6FDA, APC-6FDA, and ATPA-3FA was confirmed by $^1\text{H NMR}$, $^{13}\text{C NMR}$, and elemental analysis. The chemical shifts and peak integration of NMR spectra shown in Figure 2 are consistent with the proposed structure. Also, the experimental carbon, hydrogen, and nitrogen contents are in a good agreement with the theoretical contents. The above results suggested the successful preparation of the proposed oligoimides.

Characterization of D-A Oligoimides. The thermal, photo-physical, and electrochemical properties of D-A oligoimides are listed in Table 1. The thermal decomposition temperatures (T_d , 5% weight loss temperatures) (Figure S1a, Supporting Information) of ATPA-6FDA, APC-6FDA, and ATPA-3FA were 459, 526, and 381 $^{\circ}\text{C}$, respectively, indicating good thermal

stability of the D-A oligoimides for memory device applications. ATPC-6FDA exhibited the highest T_d value, compared to the other oligoimides, which was probably attributed to the rigid rings within the carbazole moieties. The higher T_d of ATPA-6FDA than of ATPA-3FA was probably due to the former having more triphenylamine moieties, enhancing the thermal stability. Among these oligoimides, only ATPA-3FA showed the crystalline behaviors, as shown in Figure S1b in Supporting Information. The crystalline and melting temperatures of ATPA-3FA were observed at 176 and 219 $^{\circ}\text{C}$, respectively, as shown in Supporting Information. This crystallinity of ATPA-3FA might arise from its bending structure. From the Gaussian calculation, the dipole moments of ATPA-6FDA, APC-6FDA, and ATPA-3FA were 1.54, 0.52, and 1.92 D. The bending structure of ATPA-3FA possessed higher polarity and probably resulted in a stronger intermolecular interaction, facilitating its molecular packing.

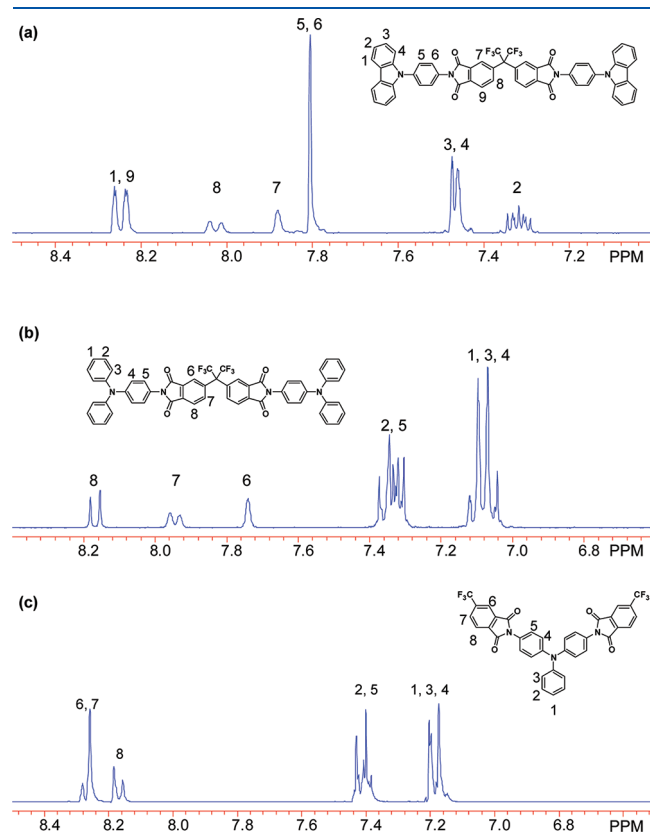


Figure 2. $^1\text{H NMR}$ spectra of (a) ATPA-6FDA, (b) APC-6FDA, and (c) ATPA-3FA.

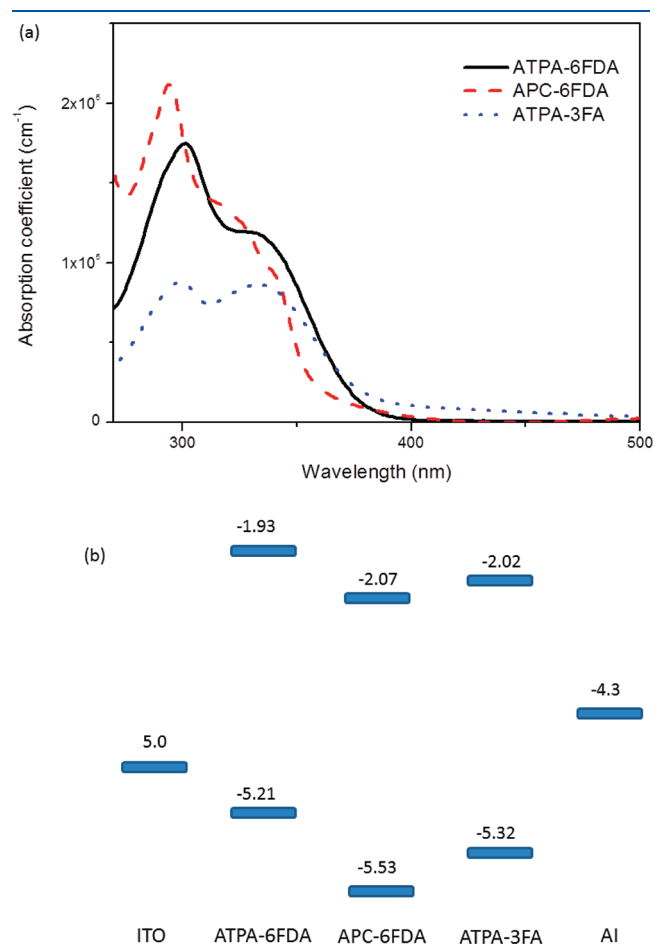


Figure 3. (a) UV–vis absorption spectra and (b) energy diagram of D-A oligoimide thin films.

Table 1. Thermal, Optical, and Electrochemical Properties of the Prepared D-A Oligoimides

oligoimide	T_d ($^{\circ}\text{C}$)	T_c ($^{\circ}\text{C}$)	T_m ($^{\circ}\text{C}$)	absorption λ_{max} (nm)	band gap ^a (eV)	HOMO (eV)	LUMO ^b (eV)
ATPA-6FDA	459			300, 333	3.28	−5.21	−1.93
APC-6FDA	526			294, 318 ^c , 333 ^c	3.51	−5.53	−2.02
ATPA-3FA	381	176	219	299, 333	3.25	−5.32	−2.07

^a Estimated from the onset of absorption. ^b LUMO = HOMO + band gap. ^c Absorption shoulders.

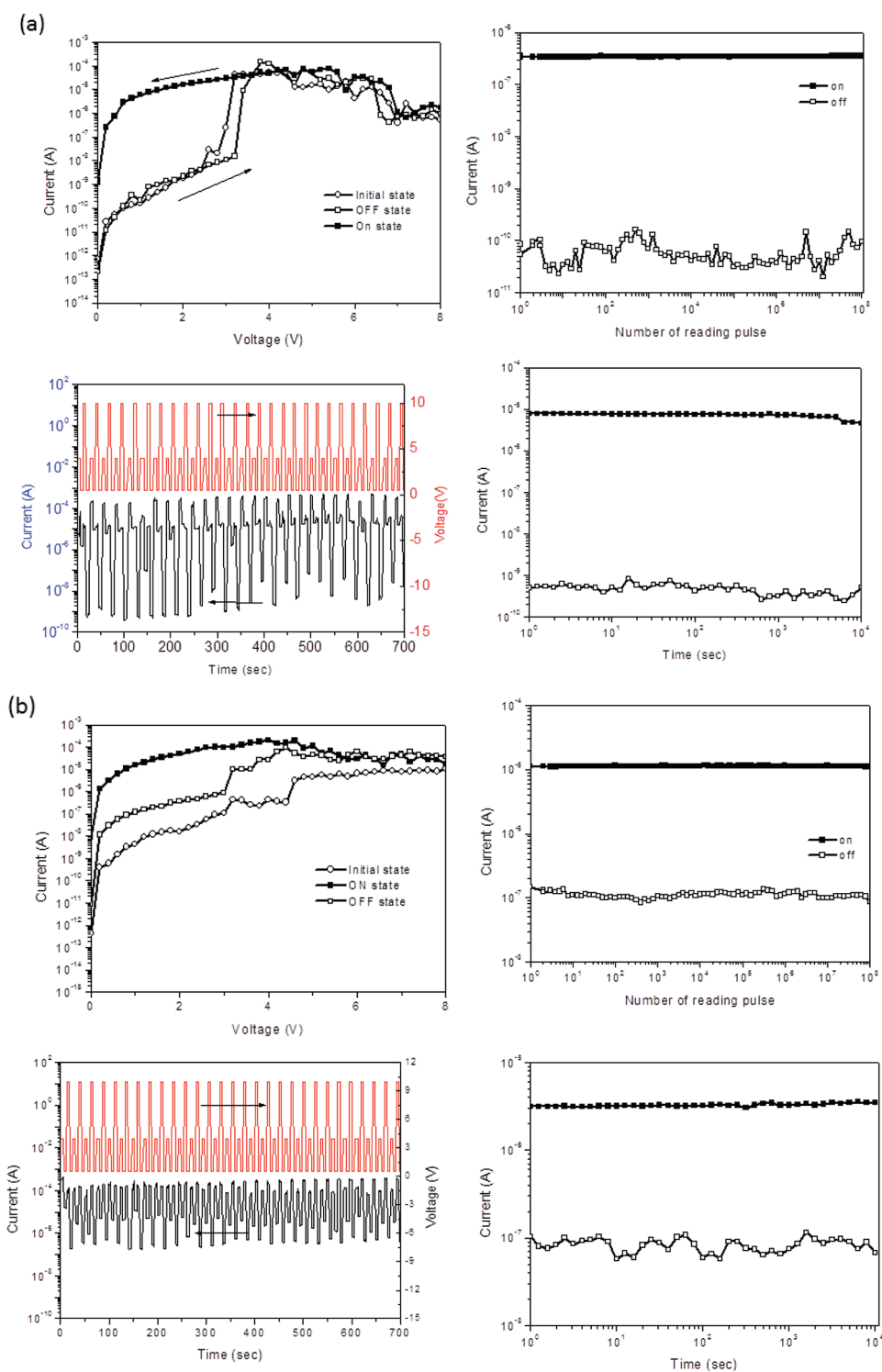


Figure 4. Electrical switching characteristics of (a) ATPA-6FDA and (b) APC-6FDA, including I – V curves, retention time, write-read-erase-read cycles, and pulse reading.

Figure 3a shows the UV–vis absorption spectra of the three D-A oligoimides in thin films on quartz substrates. The band gaps of ATPA-6FDA, APC-6FDA, and ATPA-3FA estimated from the onset of the absorption spectra were 3.28, 3.51, and 3.25 eV, respectively. The absorption maxima at 294 (4.21 eV) and 300 nm (4.13 eV) are respectively attributed to the π – π^* transition of carbazole (HOMO \rightarrow LUMOs) (4.66 eV) and

triphenylamine moieties (HOMO \rightarrow LUMO4) (4.59 eV), according to the theoretical calculation shown in Figures S2 and S3 (Supporting Information). The absorption band from 318 to 333 nm arose from the transition of charge transfer from the donor to acceptor moieties. The absorption of the D-A-D triphenylamine-based oligomers at 333 nm is stronger than that of the A-D-A oligoimides, implying that the D-A-D arrangement

provides a stronger probability of charge transfer than the A-D-A one. Thus, the D-A-D molecules probably have a higher possibility of charge transfer with neighboring molecules when the external voltage is applied.

The electrochemical properties of the oligoimides were measured by cyclic voltammetry (CV) (see Figure S4 in Supporting Information). The oxidation behaviors of the oligoimides were obtained in anhydrous acetonitrile with tetrabutylammonium perchlorate as electrolyte. The highest occupied molecular orbital (HOMO) energy levels of the oligoimides were calculated from the cyclic voltammetry with reference to ferrocene (4.8 eV) by the following equation: $\text{HOMO} = -(E^{\text{onset}} + 4.8 - E_{\text{ferrocene}})$, summarized in Table 1 and Figure 3b. The HOMO levels of ATPA-6FDA, APC-6FDA, and ATPA-3FA are -5.21 , -5.53 , and -5.32 eV, respectively. The lowest unoccupied molecular orbital (LUMO) levels are not available from CV, and thus the values of the LUMO levels were estimated from the difference between the optical band gaps and the HOMO level. Among the oligoimides, the HOMO level of ATPA-6FDA is the closest to the work function of ITO glass. This indicates that the barrier of the hole injection is the smallest, as compared to the other molecules.

Memory Characteristics of the D-A Oligoimides. The resistor-type memory of the D-A oligoimides was fabricated in a simple sandwich configuration, Al/oligoimide/ITO. Figure 4 shows the I - V electrical switching of the memory devices based on D-A-D oligoimides. The ATPA-6FDA device (Figure 4a) was initially in a low-conductance state (off state) as the voltage swept from 0 to 3 V. The current increased abruptly as a high-conductance state (on state) when the voltage was around 3 V, defined as the switching threshold voltage. As the voltage increased continuously from the threshold voltage to 4.5 V (V_{max}), the current increased. When the voltage swept to a high-voltage region around 8 V (V_{min}), the current decreased significantly as an off state. The writing and erasing process could be manipulated by applied V_{max} and V_{min} to the devices in the unipolar direction of voltage sweeping, which is defined as the negative-differential-resistance (NDR) behavior. The NDR behavior is an electrical property of devices where increased voltages induce a decrease in the current.^{4,9b} This NDR switching can produce repeatable switching many times in the same device. At least 20 devices were measured from five different batches and showed stable NDR characteristics. The stability of the memory effect was evaluated by testing the retention time, pulse reading, and write-read-erase-read (WRER) cycles, as shown in Figure 4. The retention time of the devices based on the D-A-D oligomers can maintain the on and off states longer than 10^4 s without constant stress applied in the testing. This excellent electrical stability indicates that the type of device based on the D-A-D oligoimides is a nonvolatile memory. After pulse reading of 10^8 cycles at 0.5 V, no obvious degradation in the current was observed for the on and off states. Thus, both on and off states were stable in the long-term testing and repetitive operation cycles of the reading pulse. Programmable cyclic duration was tested by repeating the WRER cycles. The writing, reading, and erasing were set to voltages of 4, 0.5, and 10 V, respectively. The duration of each sequential step was about 4 s. The responding on and off current showed good stability in the WRER testing. The stable performance of the D-A-D oligoimides provided a promising commercial potential for a wide variety of memory applications, such as a portable disk, smart label, and radio-frequency identification (RFID) tags.

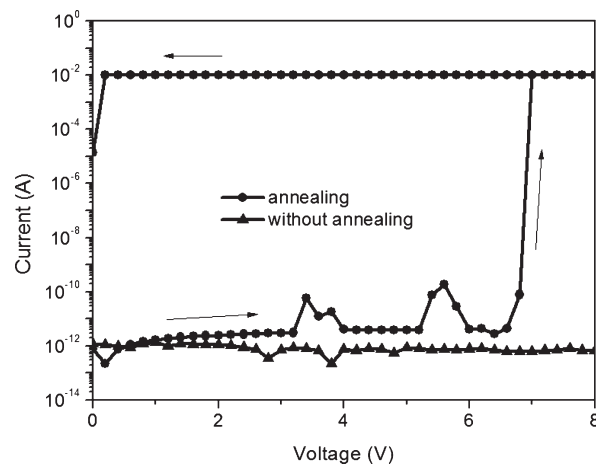


Figure 5. Electrical switching performance of ATPA-3FA with thermal treatment.

In comparison to ATPA-6FDA, APC-6FDA (Figure 4b) also showed the NDR behaviors. However, it required a relatively high voltage of 4.4 V to turn on the devices in the initial sweeping. This is presumably related to its low-lying HOMO level of 5.53 eV, resulting in a large energy barrier of ca. 0.5 eV for the hole injection. After the initial sweeping, the turn-on voltage of APC-6FDA was reduced to 3.2 V, indicating that probably some charges were trapped within the active layer, facilitating the charge injection. Triphenylamine-based ATPA-6FDA exhibited excellent unipolar electrical switching with an on/off ratio of up to 10^4 , while carbazole-based APC-6FDA showed only a poor on/off ratio of 10^1 – 10^2 . This is probably because the planar and rigid structure of carbazole moieties of APC-6FDA facilitate stacking with the adjacent carbazole moieties, resulting in enhanced charge hopping and an increase in the off current. The stacking of carbazole units is evidenced by the photoluminescence (PL) spectrum of APC-6FDA, as shown in Figure S5b of the Supporting Information.

It should be noted that only the D-A-D molecules could perform the electrical switching from a low-conducting state (off) to a high-conductance state (on), while the A-D-A molecules could not show any electrical bistability (\blacktriangle in Figure 5). This suggests that there is a large barrier for charge injection in the molecules with the A-D-A arrangement. The work function of ITO (5.0 eV) is close to the HOMO levels of the oligoimides, while Al electrode (4.3 eV) has a large mismatch of energy, ca. 2 eV, with the LUMO levels. Thus, hole injection occurs prior to electron injection, when a driving voltage is applied on the devices. In the case of A-D-A structure, it is hard for the donor to transport charges with neighboring molecules owing to the end-capping acceptor 6FDA, with a low-lying HOMO of -7.8 eV.²¹ Therefore, it is difficult for the oligoimides with the A-D-A structure to have a channel for hole carriers.

We found that thermal annealing significantly affected the electrical properties and surface morphology of ATPA-3FA. Thermal annealing can induce the crystalline behavior of ATPA-3FA. The electrical properties of ATPA-3FA showed a huge change from an insulator to a conductor after the device was annealed, as shown in Figure 5. A very large current was observed, and this may result from the formation of deep grain boundaries. During the annealing, the ATPA-3FA molecules aggregated to form a terrace morphology, as shown in Figure 6.

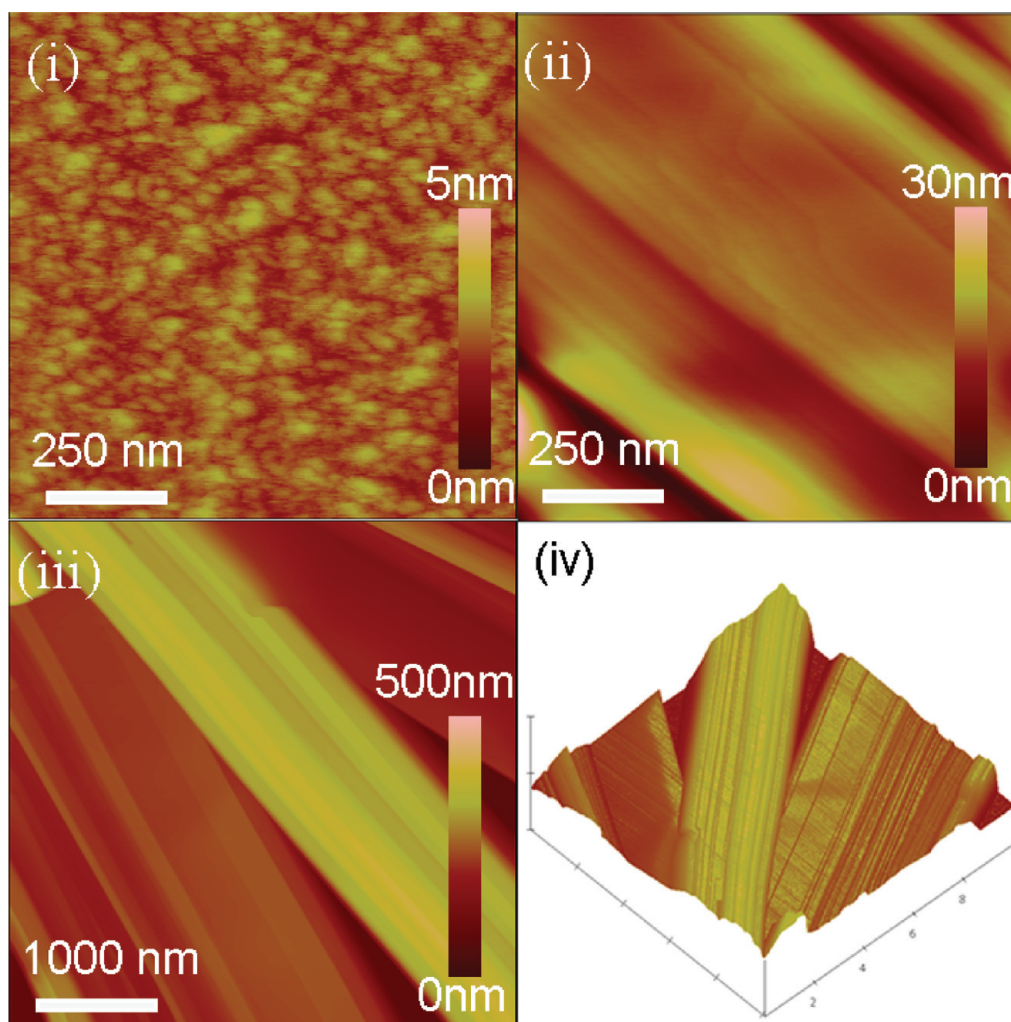


Figure 6. AFM height image of ATPA-3FA: (i) without thermal treatment; (ii, iii) with thermal annealing at 180 °C for 30 min in different scales; (iv) 3-dimensional images for the surface with thermal annealing.

The boundaries of the terrace morphology provided an effective pathway for the diffusion of the aluminum atoms. Therefore, formation of the filaments induced a very high current when the device was operating. The surface morphology of the vapor-deposited thin films of ATPA-6FDA and APC-6FDA according to AFM scanning (Figure S6, Supporting Information) showed a smooth and continuous surface with root-mean-square roughness of 0.41 and 0.39 nm, respectively. This suggests that the electrical performance of the D-A-D oligoimides may be not attributed to the formation of the aluminum filament, because there is no effective pathway for diffusion of the aluminum atoms. Besides, unlike the large influence of thermal annealing on electrical switching of the A-D-A oligoimides, the D-A-D molecules did not exhibit significant change with thermal annealing (Figure S7, Supporting Information). This is probably related to the lack of crystalline or melting temperatures in the DSC scans. Therefore, thermal annealing does not obviously affect the device performance of the D-A-D materials.

Molecular Simulation of the Oligoimides. The molecular conformation and electronic properties were explored through density functional theory. Figure 7 shows the optimized geometry, molecular orbitals and electrostatic potentials (ESP) of ATPA-6FDA and APC-6FDA, which were calculated at the

B3LYP/6-31G(d) level. HOMO orbitals are localized at the donor moieties regardless of triphenylamine or carbazole groups, while LUMO orbitals are localized at the acceptor moieties, 6FDA. This implies that the charge transfer between donor and acceptor moieties occurs in the excited state of the oligoimides. Under excitations with sufficient energy, electrons are possibly transferred from the donor moieties to the electron-withdrawing 6FDA group, while the conjugated donor moieties give a channel for the hole transporting, improving the conductivity of the oligoimides. Since the oligoimides are small molecules and not fully conjugated, the intermolecular hopping of charge carrier between neighboring donor groups dominates the charge transport. It is found that the oligoimides have negative ESP regions mainly arising from the oxygen atoms in phthalimide groups. ESP is defined as the potential energy arising from charges at the specific location.^{2a} The negative ESP region means that this region acts as a trap localizing the charge carrier, leading to charge retention and memory effects.^{3b} This supports that electrons tend to transfer to phthalimide groups from the donor moieties under excitation.

The electron of the HOMO orbital of APC-6FDA is mainly localized on the carbazole moieties and less localized on the benzene ring between the carbazole moieties and the electron-accepting

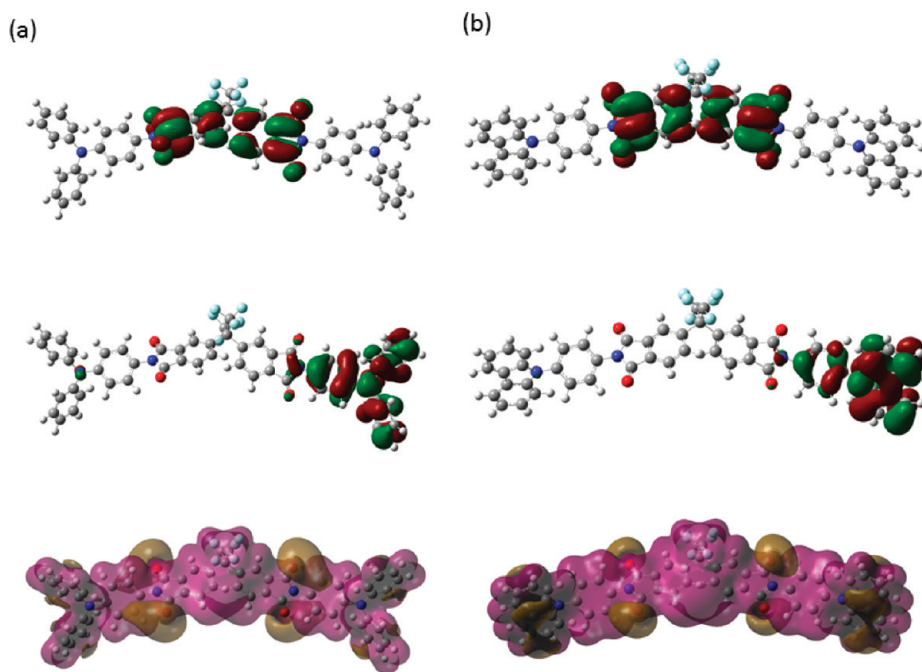


Figure 7. Molecular orbitals of the HOMO and LUMO levels and ESP surface of (a) ATPA-6FDA and (b) APC-6FDA.

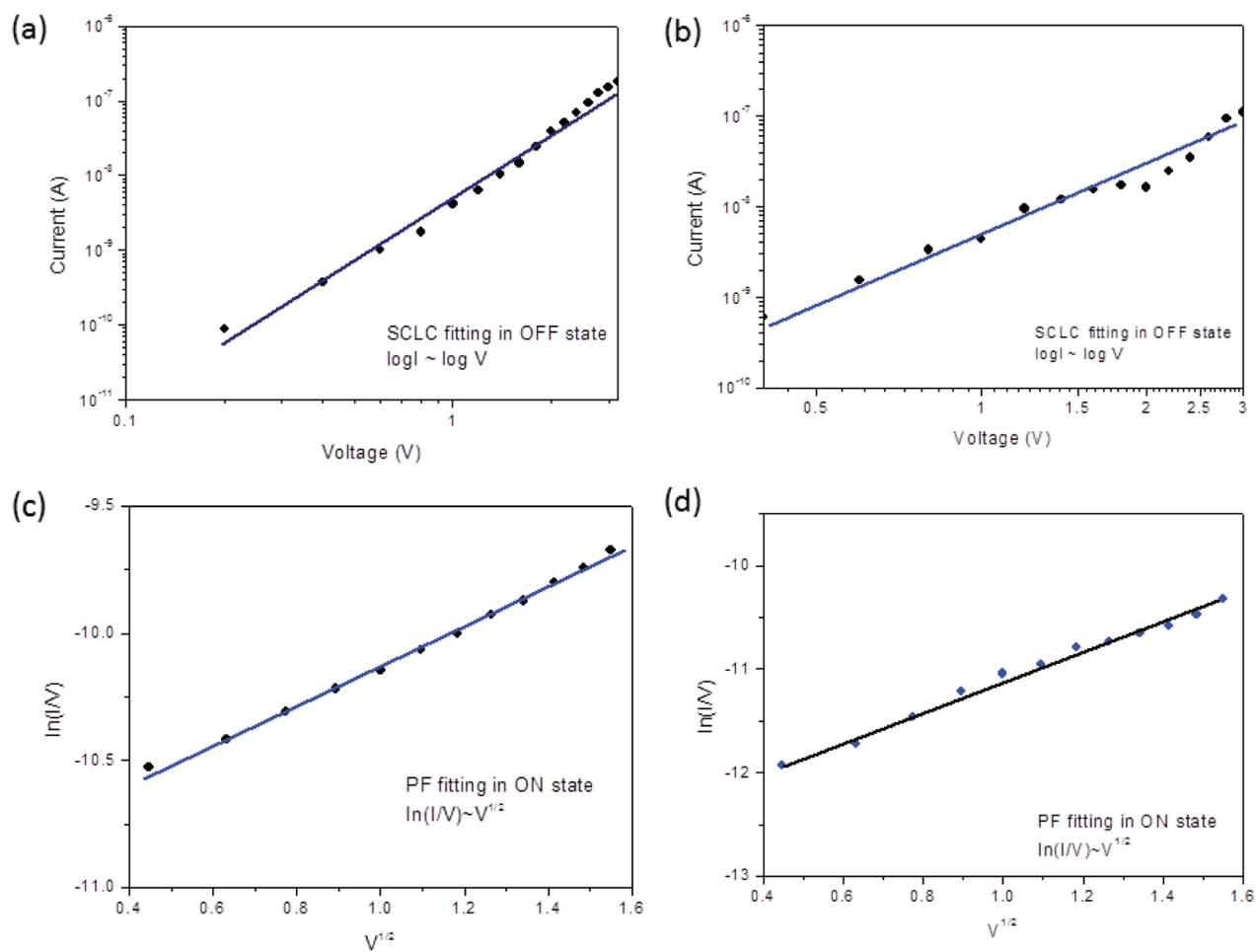


Figure 8. Analysis of $I-V$ characteristics of the off and on states of the devices based on (a, c) ATPA-6FDA and (b, d) APC-6FDA, respectively.

groups, suggesting that benzene may play a role of a spacer and hinder the charge transfer. The torsional angle between the carbazole segment and the adjacent benzene rings is 53.5° , much larger than that between the phenyl rings of triphenylamine (37°). This suggests that there is probably a large energy barrier for electrons in the transition from the excited state to the ground state of APC-6FDA. The difficult transition from LUMO to HOMO levels may also result in the residual positive charges that are still localized in the carbazole moieties when the applied voltage is turned off. This leads to the occurrence of a large off current. Besides, since ATPA-6FDA has a large conformational freedom due to the rotation of the phenyl groups, the π - π interaction of ATPA-6FDA between the adjacent triphenylamine groups is supposed to be weaker, as compared with APC-6FDA. The high conformation freedom of the flexible phenyl groups perturbed the packing of the triphenylamine groups, leading to a low tunnel current in the off state.

To further investigate the electrical behaviors of the memory devices based on the oligoimides, the measured I - V curves were analyzed by employing several theoretical models, including ohmic contact, space-charge-limited conduction (SCLC), Poole-Frenkel (PF) emission, and so on. Figure 8a,b shows the linear fitting in the logarithmic plots of I versus V for the off states of ATPA-6FDA and APC-6FDA with slopes of 2.8 and 2.4. It means that a trap-limited SCLC dominates the electrical properties in the off state because the slope is greater than 2.¹¹ On the other hand, a linear relationship was observed in a plot of $\log(I/V)$ versus $V^{1/2}$ in the on state, as shown in Figure 8c,d. It indicates that Poole-Frenkel emission dominates the high-conductive state. The PF emission is probably attributed to charge transport of organic materials filled with charge traps.¹² In the oligoimides, the electron-withdrawing 6FDA groups act as deep charge-trapping sites. The injection barriers between the ITO anode and the HOMO levels of the oligoimides are in the range of 0.2–0.53 eV, which is much smaller than the barriers between the Al cathode and LUMO levels (>2 eV). It indicates that hole injection is easier than electron injection. In the off state, hole injection occurs when the electrical field is larger than the energy barrier. Close to the threshold voltages, the carriers fill the trap sites and facilitate electron injection from the Al cathode, leading to double-carrier injection and increasing abruptly the conductivity of oligoimides. As the voltage bias is too high, the charge-filled traps induce an opposite built-in electrical field against the bias, resulting in the reduction of the conductivity. As compared to the volatile memory properties of TP6F-PI^{2d} with a similar chemical structure, the oligomer showed nonvolatile NDR behavior. As compared to the solution-processed polyimides, the oligoimides prepared from vapor deposition tend to have denser stacking and increase the intermolecular interaction with adjacent molecules, which easily induces the formation of excimers and stabilizes the trapped charges. This also supported by the photoluminescence spectrum. ATPA-6FDA exhibited a broad peak at 440 nm,¹³ as shown in Figure S5a (Supporting Information), which is attributed to excimer formation between the triphenylamine moieties. Similarly, the APC-6FDA films showed a broad PL peak at 387 nm (Figure S5b, Supporting Information), attributed to the emission of excimeric carbazole moieties.^{5e} These results indicate that these oligoimides tend to form excimers in the excited state. The intermolecular interaction within the oligoimides enhances the charge trapping and leads to nonvolatile memory characteristics.

CONCLUSIONS

We have successfully synthesized three new D-A oligoimides and demonstrated the effects of the D-A arrangement on the electrical switching behavior. The devices based on the D-A-D oligoimide with the triphenylamine segment exhibited nonvolatile NDR behavior and a high on/off ratio of 10^3 – 10^4 , while A-D-A oligoimides with the same groups showed an insulating property. The different memory characteristics were probably due to the influence of terminal hole transporting groups facilitating the injection of hole carriers. The memory devices with D-A-D oligoimides revealed repeatable nonvolatile NDR behaviors and excellent stability during operation. Moreover, the D-A-D oligoimide with the triphenylamine groups exhibited a lower off current than that with the rigid carbazole groups, because of the difficulty of the transition between HOMO and LUMO levels of the carbazole moieties. The residual positive charges were probably localized in the carbazole moieties when the applied voltage was turned off. The results provided a new strategy for designing D-A oligomers for high-performance memory device applications.

ASSOCIATED CONTENT

S Supporting Information. Seven figures showing TGA and DSC profiles and CV curves of the oligoimides ATPA-6FDA, APC-6FDA, and ATPA-3FA, molecular orbitals and AFM height and phase images of ATPA-6FDA and APC-6FDA; PL spectra of ATP-6FDA and APC-6FDA in the thin-film state; and electrical switching characteristics of ATPA-6FDA and APC-6FDA thin films after thermal annealing. This material is available free of charge via the Internet at <http://pubs.acs.org>.

AUTHOR INFORMATION

Corresponding Author

*Tel 886-2-33665236; fax 886-2-33665237; e-mail: chenwc@ntu.edu.tw (W.-C.C.) or ueda.m.ad@m.titech.ac.jp (M.U.).

Author Contributions

^{||}W.-Y.L. and T.K. contributed equally to this work.

ACKNOWLEDGMENT

Financial support from National Science Council of Taiwan, Ministry of Economic Affairs of Taiwan, and National Taiwan University Excellent Research program are highly appreciated. W.-Y. L. highly appreciates Dr. Jung-Ching Hsu for the helpful discussions of memory mechanisms.

REFERENCES

- (1) (a) Ling, Q.; Liaw, D.; Zhu, C.; Chan, D.; Kang, E.; Neoh, K. *Prog. Polym. Sci.* **2008**, *33*, 917. (b) Heremans, P.; Gelinck, G. H.; Muller, R.; Baeg, K. J.; Kim, D. Y.; Noh, Y. Y. *Chem. Mater.* **2011**, *23*, 341.
- (2) (a) Liu, Y.-L.; Wang, K.-L.; Huang, G.-S.; Zhu, C.-X.; Tok, E.-S.; Neoh, K.-G.; Kang, E.-T. *Chem. Mater.* **2009**, *21*, 3391. (b) Liu, Y.-L.; Ling, Q.-D.; Kang, E.-T.; Neoh, K.-G.; Liaw, D.-J.; Wang, K.-L.; Liou, W.-T.; Zhu, C.-X.; Chan, D. S.-H. *J. Appl. Phys.* **2009**, *105*, No. 044501. (c) Wang, K. L.; Liu, Y. L.; Shih, I. H.; Neoh, K. G.; Kang, E. T. *J. Polym. Sci., Part A: Polym. Chem.* **2010**, *48*, 5790. (d) Ling, Q. D.; Chang, F. C.; Song, Y.; Zhu, C. X.; Liaw, D. J.; Chan, D. S. H.; Kang, E. T.; Neoh, K. G. *J. Am. Chem. Soc.* **2006**, *128*, 8732. (e) Wang, K. L.; Liu, Y. L.; Lee, J. W.; Neoh, K. G.; Kang, E. T. *Macromolecules* **2010**, *43*, 7159. (f) Kuorosawa, T.; Chueh, C.-C.; Liu, C.-L.; Higashihara, T.; Ueda, M.; Chen, W.-C.

- Macromolecules* **2010**, *43*, 1236. (g) You, N. H.; Chueh, C. C.; Liu, C. L.; Ueda, M.; Chen, W. C. *Macromolecules* **2009**, *42*, 4456. (h) Hahm, S. G.; Choi, S.; Hong, S.-H.; Lee, T. J.; Park, S.; Kim, D. M.; Kwon, W.-S.; Kim, K.; Kim, O.; Ree, M. *Adv. Funct. Mater.* **2008**, *18*, 3276. (i) Tian, G. F.; Wu, D. Z.; Qi, S. L.; Wu, Z. P.; Wang, X. D. *Macromol. Rapid Commun.* **2011**, *32*, 384. (j) Liu, C. L.; Kurosawa, T.; Yu, A. D.; Higashihara, T.; Ueda, M.; Chen, W. C. *J. Phys. Chem. C* **2011**, *115*, 5930.
- (3) (a) Baek, S.; Lee, D.; Kim, J.; Hong, S. H.; Kim, O.; Ree, M. *Adv. Funct. Mater.* **2007**, *17*, 2637. (b) Ling, Q.-D.; Song, Y.; Lim, S.-L.; Teo, E. Y.-H.; Tan, Y.-P.; Zhu, C.; Chan, D. S. H.; Kwong, D.-L.; Kang, E.-T.; Neoh, K.-G. *Angew. Chem., Int. Ed.* **2006**, *45*, 2947. (c) Pearson, C.; Ahn, J. H.; Mabrook, M. F.; Zeze, D. A.; Petty, M. C.; Kamtekar, K. T.; Wang, C.; Bryce, M. R.; Dimitrakakis, P.; Tsoukalas, D. *Appl. Phys. Lett.* **2007**, *91*, No. 123506. (d) Xu, X.; Li, L.; Liu, B.; Zou, Y. *Appl. Phys. Lett.* **2011**, *98*, No. 063303.
- (4) Fang, Y.-K.; Liu, C.-L.; Li, C.; Lin, C.-J.; Mezzenga, R.; Chen, W.-C. *Adv. Funct. Mater.* **2010**, *20*, 3012.
- (5) (a) Teo, E. Y. H.; Ling, Q. D.; Song, Y.; Tan, Y. P.; Wang, W.; Kang, E. T.; Chan, D. S. H.; Zhu, C. X. *Org. Electron.* **2006**, *7*, 173. (b) Liu, C.-L.; Hsu, J.-C.; Chen, W.-C.; Sugiyama, K.; Hirao, A. *ACS Appl. Mater. Interfaces* **2009**, *1*, 1974. (c) Fang, Y. K.; Liu, C. L.; Yang, G. Y.; Chen, P. C.; Chen, W. C. *Macromolecules* **2011**, *44*, 2604. (d) Fang, Y. K.; Liu, C. L.; Chen, W. C. *J. Mater. Chem.* **2011**, *21*, 4778. (e) Lim, S. L.; Ling, Q. D.; Teo, E. Y. H.; Zhu, C. X.; Chan, D. S. H.; Kang, E. T.; Neoh, K. G. *Chem. Mater.* **2007**, *19*, 5148.
- (6) (a) Potember, R. S.; Poehler, T. O.; Cowan, D. O. *Appl. Phys. Lett.* **1979**, *34*, 405. (b) Billen, J.; Steudel, S.; Müller, R.; Genoe, J.; Heremans, P. *Appl. Phys. Lett.* **2007**, *91*, No. 263507. (c) Wu, H. M.; Song, Y. L.; Du, S. X.; Liu, H. W.; Gao, H. J.; Jiang, L.; Zhu, D. B. *Adv. Mater.* **2003**, *15*, 1925. (d) Shang, Y. L.; Wen, Y. Q.; Li, S. L.; Du, S. X.; He, X. B.; Cai, L.; Li, Y. F.; Yang, L. M.; Gao, H. J.; Song, Y. *J. Am. Chem. Soc.* **2007**, *129*, 11674. (e) Ma, Y.; Cao, X.; Li, G.; Wen, Y.; Yang, Y.; Wang, J.; Du, S.; Yang, L.; Gao, H.; Song, Y. *Adv. Funct. Mater.* **2010**, *20*, 803. (f) Ouyang, M.; Hou, S. M.; Chen, H. F.; Wang, K. Z.; Xue, Z. Q. *Phys. Lett. A* **1997**, *235*, 413. (g) Mukherjee, B.; Pal, A. J. *Chem. Mater.* **2007**, *19*, 1382.
- (7) (a) Zhuang, X. D.; Chen, Y.; Liu, G.; Li, P. P.; Zhu, C. X.; Kang, E. T.; Neoh, K. G.; Zhang, B.; Zhu, J. H.; Li, Y. X. *Adv. Mater.* **2010**, *22*, 1731. (b) Liu, G.; Zhuang, X. D.; Chen, Y.; Zhang, B.; Zhu, J. H.; Zhu, C. X.; Neoh, K. G.; Kang, E. T. *Appl. Phys. Lett.* **2009**, *95*, No. 253301. (c) Li, G. L.; Liu, G.; Li, M.; Wan, D.; Neoh, K. G.; Kang, E. T. *J. Phys. Chem. C* **2010**, *114*, 12742.
- (8) Song, S.; Cho, B.; Kim, T.-W.; Ji, Y.; Jo, M.; Wang, G.; Choe, M.; Kahng, Y. H.; Hwang, H.; Lee, T. *Adv. Mater.* **2010**, *22*, 5048.
- (9) (a) Ouyang, J.; Chu, C.-W.; Szmanda, C. R.; Ma, L.; Yang, Y. *Nat. Mater.* **2004**, *3*, 918. (b) Scott, J. C.; Bozano, L. D. *Adv. Mater.* **2007**, *19*, 1452. (c) Ouyang, J.; Chu, C.-W.; Sieves, D.; Yang, Y. *Appl. Phys. Lett.* **2005**, *86*, No. 123507.
- (10) Frisch, M. J.; Trucks, G. W.; Schlegel, H. B.; Scuseria, G. E.; Robb, M. A.; Cheeseman, J. R.; Montgomery, J. A., Jr.; Vreven, T.; Kudin, K. N.; Burant, J. C.; Millam, J. M.; Iyengar, S. S.; Tomasi, J.; Barone, V.; Mennucci, B.; Cossi, M.; Scalmani, G.; Rega, N.; Petersson, G. A.; Nakatsuji, H.; Hada, M.; Ehara, M.; Toyota, K.; Fukuda, R.; Hasegawa, J.; Ishida, M.; Nakajima, T.; Honda, Y.; Kitao, O.; Nakai, H.; Klene, M.; Li, X.; Knox, J. E.; Hratchian, H.; P.; Cross, J. B.; Bakken, V.; Adamo, C.; Jaramillo, J.; Gomperts, R.; Stratmann, R. E.; Yazyev, O.; Austin, A. J.; Cammi, R.; Pomelli, C.; Ochterski, J. W.; Ayala, P. Y.; Morokuma, K.; Voth, G. A.; Salvador, P.; Dannenberg, J. J.; Zakrzewski, V. G.; Dapprich, S.; Daniels, A. D.; Strain, M. C.; Farkas, O.; Malick, D. K.; Rabuck, A. D.; Raghavachari, K.; Foresman, J. B.; Ortiz, J. V.; Cui, Q.; Baboul, A. G.; Clifford, S.; Cioslowski, J.; Stefanov, B. B.; Liu, G.; Liashenko, A.; Piskorz, P.; Komaromi, I.; Martin, R. L.; Fox, D. J.; Keith, T.; Al-Laham, M. A.; Peng, C. Y.; Nanayakkara, A.; Challacombe, M.; Gill, P. M. W.; Johnson, B.; Chen, W.; Wong, M. W.; Gonzalez, C.; Pople, J. A. *Gaussian 03, revision B.04*, Gaussian, Inc., Wallingford, CT, 2004.
- (11) Hahm, S. G.; Choi, S.; Hong, S. H.; Lee, T. J.; Park, S.; Kim, D. M.; Kwon, W. S.; Kim, K.; Kim, O.; Ree, M. *Adv. Funct. Mater.* **2008**, *18*, 3276.
- (12) (a) Chu, C. W.; Ouyang, J.; Tseng, H. H.; Yang, Y. *Adv. Mater.* **2005**, *17*, 1440. (b) Hsu, J.-C.; Liu, C.-L.; Chen, W.-C.; Sugiyama, K.; Hirao, A. *Macromol. Rapid Commun.* **2011**, *32*, 528.
- (13) (a) Hsu, J.-C.; Chen, Y.; Kakuchi, T.; Chen, W.-C. *Macromolecules* **2011**, *44*, 5168. (b) Fang, Y. K.; Lee, W. Y.; Tuan, C. S.; Lu, L. H.; Teng, W. J.; Chen, W. C. *Polym. J.* **2010**, *42*, 327.